Comparative study of the optical properties of single-walled carbon nanotubes within orthogonal and nonorthogonal tight-binding models

Valentin N. Popov* and Luc Henrard
Laboratoire de Physique du Solide, Facultés Universitaires Notre-Dame de la Paix, Rue de Bruxelles, 61. B-5000 Namur, Belgium
(Received 5 February 2004; revised manuscript received 13 May 2004; published 13 September 2004)

The dielectric response function of single-walled carbon nanotubes is calculated within tight-binding models with different levels of complexity. First, the effects of the orbital basis set of the model, the orbitals overlap, and the structural optimization on the electronic band structure and the dielectric function of three small-radius nanotubes are investigated in detail. Second, the optical transition energies for a large number of nanotubes are derived from the peak positions of the imaginary part of the dielectric function for parallel and perpendicular light polarization. These results can be useful for the assignment of absorption spectra of nanotube samples and for the determination of the conditions for resonant Raman scattering from nanotubes. The obtained results are compared to recent spectrofluorimetric data on isolated single-walled carbon nanotubes.

DOI: 10.1103/PhysRevB.70.115407 PACS number(s): 78.67.−n, 73.22.−f, 61.46+w

I. INTRODUCTION

Since the discovery of the carbon nanotubes in 1991[1] significant efforts have been directed toward their experimental and theoretical investigation inspired by the speculations about their amazing properties.[2] The simplest nanotube is a single graphitic layer (graphene) wrapped seamlessly into a cylinder and is called the single-walled nanotube (SWNT or, simply, nanotube). It can be characterized uniquely by a pair of integer numbers (L_1, L_2). The electronic structure of any nanotube can be obtained within the π-band tight-binding model of graphene (π-TB model) by folding the π-band along a certain direction in the two-dimensional Brillouin zone.[3] In this approach, it is predicted that a nanotube is a metal if $L_1 - L_2$ is a multiple of 3 or a semiconductor otherwise. Band structure calculations within an all-valence nonorthogonal tight-binding model[4] revealed that nanotubes with $L_1 - L_2 = 3n$ $(n = 1, 2, \ldots,)$ are very-small-gap semiconductors. A similar model based on a symmetry-adapted scheme[5] was used for band structure calculations of a number of nanotubes. The electronic structure of nanotubes can be predicted with high accuracy by *ab initio* calculations. Using a plane-wave *ab initio* pseudopotential local-density-functional (LDA) approach, [6] it was possible to study in more detail the curvature-induced σ- and π-band mixing and the deviation from the sp^2 hybridization. In particular, these effects were found to alter significantly the electronic structure of narrow nanotubes compared to the predictions of the π-TB model.[6] In the case of small-radius insulating nanotubes, due to strong $\sigma^* - \pi^*$ rehybridization, strongly modified low-lying nondegenerate conduction band states are introduced into the band gap thus lowering the gap down to 50%. Similar effects were observed in the electronic properties of carbon nanotubes with polygonized cross section calculated within a plane-wave *ab initio* pseudopotential LDA approach.[7] LDA calculations on the narrowest nanotube (5,0) revealed total closure of the gap.[8,9] By extensive LDA calculations it was shown that even for nanotubes with moderate radii R ($0.5\ \text{nm} < R < 0.75\ \text{nm}$) the energy bands are shifted by ~ 0.1 eV relative to the π-TB ones.[10]

The theoretical optical transition energies of nanotubes are of primary importance for the assignment of the peaks in the optical absorption spectra and for the interpretation of the resonant Raman spectra of nanotube samples. Most of the work on optical properties of nanotubes was based on the use of the π-TB model. The selection rules for allowed dipole transitions were first discussed by Ajiki and Ando.[11] The dielectric function of nanotubes was calculated in the random phase approximation and the gradient approximation was used for the matrix elements of the momentum. [12] A theoretical study on the optical properties of several nanotubes encompassed optical absorption, optical rotatory power, and circular dichroism and, in particular, the parallel and perpendicular (with depolarization effects) dielectric function.[13] The optical transition energies of all nanotubes with diameters between 0.6 and 1.8 nm for energies up to 3.5 eV were derived from the separations between the mirror-image spikes of the π-TB electronic density of states.[14] The π-TB transition energies were corrected for curvature effects by introducing a chirality- and diameter-dependent nearest-neighbor hopping integral in the π-TB model.[15] A precise description of the curvature effects on the optical properties was accomplished within all-valence symmetry-adapted TB models[5,16,17] and *ab initio* models.[8,9] Up to now, however, high-precision results for the optical transitions have been reported only for a relatively small number of nanotubes while for the purpose of sample characterization the theoretical optical transitions for all experimentally observed nanotubes are needed.

The experimentally observed absorption and Raman scattering spectra are currently assigned using the predictions of the π-TB models[14] and, rarely, using improved π-TB models.[15] The first and second lowest peaks in the optical absorption spectrum of purified SWNT thin films were found to correspond to the density of state (DOS) peaks of semiconducting tubes and the third one—to the DOS of metallic tubes.[14] The reflectance spectrum of an unaligned mat of SWNTs in the range 0.003−3 eV exhibited several peaks which were assigned to several nanotubes.[18] The detailed analysis of the optical properties of laser-ablation-produced

SWNTs, based on measurements of the optical absorption and high-resolution electron energy-loss spectroscopy in transmission, allowed the determinination of the mean diameter and diameter distribution in the SWNT samples.[19] Absorption spectra with well-resolved spectral features in mixed samples of individual SWNTs were assigned to transitions in specific tube type by means of an improved π-TB model.[15] Polarized optical absorption spectra of single-walled nanotubes of 4 Å diameter grown in the channels of an $AlPO_4-5$ single crystal were reported.[20] The observed three bands in the spectra for parallel polarization of the incident light were assigned to tubes (5,0), (3,3), and (4,2) by using *ab initio* predictions. In cross polarization the nanotubes were nearly transparent in the measured region 0.5–4.1 eV which was attributed to strong depolarization effects.[9]

By exciting semiconducting tubes between the second pair of van Hove singularities followed by fluorescence between the first pair of van Hove singularities, absorption and bright fluorescence from isolated SWNTs were observed.[21] This experimental technique was applied in a systematical spectrofluorimetric investigation of SWNTs, isolated in aqueous surfactant suspensions, and the absorption and emission transitions of 33 different semiconducting tubes were derived.[22] The combined fluorescence and Raman spectroscopy study of a few isolated SWNTs allowed for the precise correlation between the experimental data and the structure of the tubes.[23] SWNTs prepared by laser vaporization, dispersed and surfactant stabilized, showed photoluminescence peaks corresponding to the lowest electronic interband transitions in semiconducting tubes.[24] The obtained data in Ref. 22 were fitted to empirical expressions which were then used to obtain model-independent predictions for the first and second van Hove optical transitions (E_{11} and E_{22}) as a function of the tube structural parameters for a wide range of semiconducting tubes.[25] The derived empirical relations were found to overestimate the π-TB results for E_{11} and E_{22} up to 25%. This was attributed to a combination of effects such as trigonal warping, curvature, and exciton binding. While the first two effects can be well described within the band structure picture: modified π-TB models,[15] all-valence tight-binding models,[5,16,17] and *ab initio* models,[8,9] the description of the excitonic effects requires a different approach.[26,27] It can be concluded that the recent experimental results question the assignment of the spectroscopic data based on π-TB models, as well as on more advanced tight-binding and *ab initio* models. Therefore, it is important to perform large-scale precise band structure calculations and to compare the obtained results for the optical transitions to the optical and spectrofluorimetric data in order to gain deeper insight on the nature of the disagreement between them.

Here the dielectric function for parallel and perpendicular light polarization of a large number of nanotubes in the radius range from 2 to 15 Å is calculated within a π-TB model and two all-valence TB models using four valence electrons per carbon atom: an orthogonal TB (*o*-TB) model and a nonorthogonal TB (*n*-TB) model. The *n*-TB model is based on a symmetry-adapted scheme[28] that allows for great reduction of the computational time. It is shown that the use of all four valence electrons of carbon in the *o*-TB model instead of a single π-band introduces curvature-induced rehybridization corrections to the electronic band structure. Additionally, the accounting for orbitals overlap in the *n*-TB model leads to a better description of the effect of the curvature on the electron band structure than by the *o*-TB model. It is demonstrated that the *n*-TB model yields predictions for the band structure that are close to those of the *ab initio* models for energies up to a few electron volts around the Fermi level. The optical transition energies are derived from the positions of the peaks of the imaginary part of the dielectric function and are presented versus nanotube radius in charts. These charts can be used for the assignment of the features in the optical absorption spectra and for clarifying the conditions for resonant Raman scattering of light from nanotubes. The paper is arranged as follows. First, the nanotube structure, the TB models, and the dielectric function are introduced in Sec. II. The results of the structural optimization of a number of nanotubes and the calculations of the band structure and the dielectric function for three small-radius nanotubes, and the derived charts of the optical transition energies for parallel and perpendicular light polarization are presented and discussed in Sec. III. The paper ends with conclusions (Sec. IV).

II. THEORETICAL PART

A. Nanotube structure

The nanotube can be viewed as obtained by rolling up of an infinite strip of graphene with width defined by the chiral vector $\mathbf{C}_h = L_1\mathbf{a}_1 + L_2\mathbf{a}_2$ ($\mathbf{a}_1$ and $\mathbf{a}_2$ are the primitive translation vectors of graphene) into a seamless cylinder.[3–5] The integer numbers L_1 and L_2 ($L_1 \geqslant L_2 \geqslant 0$) uniquely specify the nanotube. Tubes with $L_1 = L_2$ ("armchair" tubes) or $L_1 \neq L_2 = 0$ ("zigzag" tubes) are termed achiral and the remaining tubes are termed chiral. The nanotube can alternatively be described by its radius R and chiral angle θ which is the angle between the chiral vector and the nearest zigzag of carbon-carbon bonds. All nanotubes have a specific symmetry defined by two different screw operators. A screw operator S_i executes a rotation at a given angle φ_i around the tube axis and a translation at a given distance t_i along the tube axis ($i = 1, 2$). A combination of screw operators $S_1^{l_1} S_2^{l_2}$ [denoted for brevity as $S(\mathbf{l})$] leads to coincidence of the zeroth lattice point of the tube with the lattice point with index $\mathbf{l} = (l_1, l_2)$. Accepting the same two-atom unit cells for the nanotube as for graphene, the unit cell at the origin can be mapped onto the entire tube by means of operators $S(\mathbf{l})$. The second atom in each two-atom unit cell can be obtained by application on the first atom of a third screw operator with a rotation angle φ' and a translation period t'.[5,28]

The rolled-up nanotube has a translational symmetry with a translation period T given by the length of the graphene lattice vector $N_1\mathbf{a}_1 + N_2\mathbf{a}_2$ where

$$N_1 = (L_1 + 2L_2)/d, \tag{1}$$

$$N_2 = -(2L_1 + L_2)/d. \tag{2}$$

Here d is equal to the highest common divisor d' of L_1 and L_2 if $L_1 - L_2$ is not a multiple of $3d'$ or d is equal to $3d'$ if

L_1-L_2 is a multiple of $3d'$. Each nanotube contains N_c atomic pairs and $N_a=2N_c$ atoms in the unit cell where

$$N_c = 2(L_1^2 + L_1L_2 + L_2^2)/d. \tag{3}$$

The parameters of the three screw operators can be expressed as

$$\varphi_1 = 2\pi N_2/N_c, \tag{4}$$

$$\varphi_2 = -2\pi N_1/N_c, \tag{5}$$

$$\varphi' = 2\pi(N_1 - N_2)/3N_c, \tag{6}$$

$$t_1 = L_2T/N_c, \tag{7}$$

$$t_2 = -L_1T/N_c, \tag{8}$$

$$t' = (L_1 - L_2)T/3N_c. \tag{9}$$

The rolled-up nanotube structure can serve as an input for structural optimization of the nanotube. It is important to note that the optimized structure of chiral tubes may not have translational symmetry. Here, such a symmetry is assumed for conformity with other studies and because the deviation of the optimized structure from the optimized structure with imposed translational periodicity is usually very small. We also assume that the screw symmetry of the tube is preserved. Therefore, Eqs. (4), (5), (7), and (8) will be still valid, but Eqs. (6) and (9) may no longer be applicable. As independent structural parameters we can choose R, T, t', and φ'. The radius R_0, translation period T_0, and chiral angle θ_0 for the rolled-up structure are given by the relations

$$R_0 = \sqrt{3(L_1^2 + L_1L_2 + L_2^2)}a_{\text{C-C}}/2\pi, \tag{10}$$

$$T_0 = 2\sqrt{3}\pi R_0/d, \tag{11}$$

$$\theta_0 = \tan^{-1}(\sqrt{3}L_2/(L_2 + 2L_1)). \tag{12}$$

Here $a_{\text{C-C}}$ is the carbon-carbon bond length for graphene. The chiral angle θ for the optimized structure can be expressed by means of the optimized R and T as $\theta = \tan^{-1}(-L_2T/2\pi N_2R)$. In Sec. III A, the obtained relative changes of R, T, and θ are discussed.

B. Tight-binding models

The screw symmetry of the nanotubes allows for the construction of a tight-binding model that is based on a two-atom unit cell rather than on the translational unit cell with N_c two-atom unit cells.[5,29] Such a symmetry-adapted tight-binding model has advantages with respect to computational time and resources that will be discussed below.

In the independent-electron approximation, the one-electron wave functions of a nanotube $\psi_{kl}(\mathbf{r})$ are labeled by the one-dimensional wave vector $k(-\pi \leqslant k \leqslant \pi)$ and the discrete quantum number $l(l=0,1,\ldots,N_c-1)$ as a consequence of the rotational and translational symmetry of the nanotubes. These wave functions can be represented as linear combinations of basis functions $\varphi_{klr}(\mathbf{r})$. In the tight-binding method, the basis functions are expressed by atomic orbitals $\chi_r(\mathbf{R}(\mathbf{l})-\mathbf{r})$. The orbitals are centered on atoms with position vectors $\mathbf{R}(\mathbf{l})$. The index r runs over the orbitals on all atoms in the two-atom unit cell. For example, in the case of n orbitals per carbon atom, $r=1,2,\ldots,2n$ ($n=1$ for the π-TB model and $n=4$ for the all-valence TB models). The basis functions satisfy a generalized Bloch theorem for any screw operator $S(\mathbf{l})$

$$\sum_{r'} T_{rr'}(\mathbf{l})\varphi_{klr'}(\mathbf{r}) = e^{i[\alpha(\mathbf{l})l+z(\mathbf{l})k]}\varphi_{klr}(\mathbf{r}). \tag{13}$$

Here $T_{rr'}(\mathbf{l})$ are the matrices of the representation of the symmetry group of the screw operators $S(\mathbf{l})$ in the space of the basis functions; $\alpha(\mathbf{l})=2\pi(l_1N_2-l_2N_1)/N_c$ and $z(\mathbf{l})=(L_1l_2-L_2l_1)/N_c$ are the dimensionless coordinates of the origin of the $\mathbf{l}$th cell along the circumference and along the tube axis, respectively. Consequently, the basis functions can be cast in the Bloch form

$$\varphi_{klr}(\mathbf{r}) = \frac{1}{\sqrt{N}}\sum_{\mathbf{l}r'} e^{i[\alpha(\mathbf{l})l+z(\mathbf{l})k]}T_{rr'}(\mathbf{l})\chi_{r'}[\mathbf{R}(\mathbf{l}) - \mathbf{r}], \tag{14}$$

where N is the number of two-atom unit cells in the tube and the summation over $\mathbf{l}$ is carried out over these two-atom unit cells. Using the representation for the electron wave function $\psi_{kl}(\mathbf{r})$ as a linear combination of φ's

$$\psi_{kl}(\mathbf{r}) = \sum_r c_{klr}\varphi_{klr}(\mathbf{r}) \tag{15}$$

in the one-electron equation of Schrödinger $\hat{H}\psi_{kl}=E_{kl}\psi_{kl}$, one obtains the matrix equation for the coefficients c_{klr}

$$\sum_{r'} (H_{klrr'} - E_{kl}S_{klrr'})c_{klr'} = 0, \tag{16}$$

where

$$H_{klrr'} = \sum_{\mathbf{l}r''} e^{i(\alpha(\mathbf{l})l+z(\mathbf{l})k)}H_{rr''}(\mathbf{l})T_{r''r'}(-\mathbf{l}) \tag{17}$$

and

$$S_{klrr'} = \sum_{\mathbf{l}r''} e^{i(\alpha(\mathbf{l})l+z(\mathbf{l})k)}S_{rr''}(\mathbf{l})T_{r''r'}(-\mathbf{l}). \tag{18}$$

Here, the matrix elements of the Hamiltonian $H_{rr'}(\mathbf{l})$ and the overlap matrix elements $S_{rr'}(\mathbf{l})$ are defined by

$$H_{rr'}(\mathbf{l}) = \int d\mathbf{r}\chi_r[\mathbf{R}(0) - \mathbf{r}]\hat{H}\chi_{r'}[\mathbf{R}(\mathbf{l}) - \mathbf{r}] \tag{19}$$

and

$$S_{rr'}(\mathbf{l}) = \int d\mathbf{r}\chi_r[\mathbf{R}(0) - \mathbf{r}]\chi_{r'}[\mathbf{R}(\mathbf{l}) - \mathbf{r}]. \tag{20}$$

In the orthogonal tight-binding models, the overlap of the atomic orbitals centered on different atoms is ignored and $S_{rr'}(\mathbf{l})$ is approximated by a unit matrix. However, it is clear that the overlap of orbitals on different atoms is not always

negligible and that it may have an effect on the band structure. The overlap is included in the nonorthogonal tight-binding models.

The solutions of Eq. (16) are the electronic energies $E_{klm}$and the expansion coefficients c_{klmr}, $m=1,2,\ldots,2n$. For each k, this equation has to be solved for all values of l, i.e., N_c times. Therefore, the computational time for solving the eigenvalue problem for each k by standard diagonalization techniques scales as $(2n)^3N_c$ in the symmetry-adapted TB scheme and as $(2nN_c)^3$ in any nonsymmetry-adapted TB scheme. The advantage of the former is obvious and it makes possible large-scale calculations of the dielectric function of nanotubes where a sampling of a large number of wave vectors is required for the numerical integration over the one-dimensional Brillouin zone of the nanotube.

Finally, the total energy of a nanotube (per unit cell) E is given by

$$E = \sum_{klm}^{occ} E_{klm} + \frac{1}{2}\sum_{ij} \phi(r_{ij}), \tag{21}$$

where the first term is the band energy (the summation is over all occupied states) and the second term is the repulsive energy expressed by pair potentials $\phi(r_{ij})$ between atoms i and j. From Eq. (21), the force $\mathbf{F}$ acting on an atom with a position vector $\mathbf{R}$ can be found in the form

$$\mathbf{F} = -\sum_{klm}^{occ} c^*_{klmr}\frac{\partial(H_{klrr'} - E_{klm}S_{klrr'})}{\partial \mathbf{R}}c_{klmr'} - \frac{1}{2}\sum_{ij}\frac{\partial\phi(r_{ij})}{\partial \mathbf{R}}, \tag{22}$$

where the Hellmann-Feynman theorem is used for the band contribution to the force.

C. Dielectric function

In the process of absorption of incident on the nanotube electromagnetic radiation, electrons are excited from occupied states (v) into empty states (c). In the random-phase approximation and neglecting the local field corrections, the imaginary part of the dielectric function for direct dipole transitions and radiation polarized in the μ-direction is given as a function of the photon energy $\hbar\omega$ as[30].

$$\varepsilon_2 = \frac{4\pi^2e^2}{m^2\omega^2}\sum_{l'clv}\frac{2}{2\pi}\int dk|p_{kl'cklv,\mu}|^2\delta(E_{kl'c} - E_{klv} - \hbar\omega). \tag{23}$$

Here, e is the elementary charge, m is the electron mass, and E_{klv} and $E_{kl'c}$ are energies of occupied and empty electronic states, respectively. The matrix element of the μ-component of the operator of the linear momentum $\hat{\mathbf{p}}$

$$p_{kl'cklv,\mu} = \int d\mathbf{r}\psi^*_{kl'c}(\mathbf{r})\hat{p}_\mu\psi_{klv}(\mathbf{r}) \tag{24}$$

can be cast in the form

$$p_{kl'cklv,\mu} = f_{ll',\mu}\sum_{rr'} c^*_{kl'cr'}c_{klvr}\sum_{\mathbf{l}r''} e^{i[\alpha(\mathbf{l})l+z(\mathbf{l})k]}p_{r'r'',\mu}(\mathbf{l})T_{r''r}(-\mathbf{l}). \tag{25}$$

Here $p_{r'r'',\mu}(\mathbf{l})$ is the matrix element of $\hat{p}_\mu$ between atomic orbitals given by an expression similar to Eqs. (19) and (20). The quantities $f_{ll',\mu}$ are defined as follows: $f_{ll',x}=f_{ll',y}=(\delta_{l',l+1}+\delta_{l',l-1})/2$ and $f_{ll',z}=\delta_{ll'}$ (the z axis is chosen along the tube; $\delta_{ll'}$ is Kronecker delta). From Eq. (25), the selection rules for direct dipole transitions follow: allowed are only transitions with $l'=l$ for parallel light polarization and $l'=l\pm1$ for perpendicular polarization. This general result includes as a particular case the π-TB result of Ref. 11. If the atomic orbitals of carbon χ_r are known, the matrix elements of the momentum can be calculated from Eq. (25). In most tight-binding models, the atomic orbitals are unknown and this difficulty is usually circumvented by the so-called gradient approximation,[31] where, by using the operator relation $\hat{\mathbf{p}}=im/\hbar[\hat{H},\hat{\mathbf{r}}]$, the matrix element of the momentum is obtained as

$$p_{kl'cklv,\mu} = i\frac{m}{\hbar}f_{ll',\mu}\sum_{rr'} c^*_{kl'cr'}c_{klvr}\sum_{\mathbf{l}r''} e^{i[\alpha(\mathbf{l})l+z(\mathbf{l})k]}[R_\mu(\mathbf{l}) - R_\mu(0)]H_{r'r''}(\mathbf{l})T_{r''r}(-\mathbf{l}). \tag{26}$$

This expression excludes, however, intra-atomic contributions that can be important in some cases.[32]

III. RESULTS AND DISCUSSION

A. Optimized nanotube structure

Here, we carried out structural optimization of all 187 nanotubes in the radius range $2\text{Å}<R<15$ Åand $N_a<800$ within the n-TB model. The parameters of the n-TB model were taken from a LDA study of carbon clusters[33] where they were shown to have excellent performance in the calculation of the equilibrium lattice parameters and the cohesive energy of graphite. The n-TB electronic structure of graphene corresponds well to *ab initio* results in the range from −3 to 3 eV around the Fermi energy. This implies that the optical properties of graphene as well as those of the nanotubes should be reproduced well at least up to about 3 eV. As independent parameters in the optimization procedure were chosen R, T, φ', and t'.

The careful study of the convergence of the total energy and forces on atoms revealed that a large number of k-points was necessary for narrow tubes [e.g., for the tube (3,3) nearly 60 k-points had to be considered] and that this number was smaller for larger tubes [e.g., 30 k-points were enough for the tube (9,9)]. It was found that the minimal numbers N_k of k-points for a small number of achiral and chiral tubes with radii in the considered range lie on a monotonous curve only when drawn as a function of N_c. To explain this, we recall that the nanotube band structure can be obtained from that of graphene by folding it N_c times along a certain direction. The folded curves will become flatter and will a require a lesser number of k-points with the increase of N_c. The fit of N_k versus N_c yielded the relation $N_k \approx 200/N_c^{0.65}$ that was further

TABLE I. Calculated bond lengths (first lines) and bond angles (second lines) for three small-radius tubes in comparison with the nonoptimized ones and *ab initio* results (Ref. 8).

	Bond lengths (in Å) and bond angles (in rad)		
Tube	Nonoptimized[8]	Ref. 8	This work
(5, 0)	1.407, 1.407, 1.425	1.450, 1.450, 1.412	1.453, 1.453, 1.402
	120.4, 120.4, 110.2	119.8, 119.8, 111.2	119.4, 119.4, 111.9
(3, 3)	1.423, 1.423, 1.396	1.438, 1.438, 1.433	1.442, 1.442, 1.439
	115.6, 115.6, 120.3	118.7, 118.7, 116.2	117.0, 117.0, 116.9
(4, 2)	1.420, 1.399, 1.425	1.443, 1.440, 1.421	1.446, 1.431, 1.422
	118.7, 120.4, 113.3	118.7, 118.7, 114.1	119.0, 118.3, 114.2

used for all tubes. The maximal residual force on the separate atoms was set to 0.001 eV/Å.

The results of the structural optimization show that with respect to the rolled-up nanotube structure the nanotubes widen laterally and shorten in length, which has as a consequence a decrease of the chiral angle. This effect depends on the nanotube radius and chirality. In particular, the relative changes $\Delta R/R_0$, $|\Delta T/T_0|$, and $|\Delta\theta/\theta_0|$ are large for small radii and tend to zero with the increase of the radius. $\Delta R/R_0$ versus R_0 has the largest values close to 5% for small radii. It is almost independent on chirality and can be fitted by the power law $0.202/R_0^{2.295}$. $|\Delta T/T_0|$ is below 1% but shows a wide spread mainly for radii smaller than 8 Å. It is negligible for armchair tubes, larger for zigzag tubes and, for chiral tubes, it increases with the increase of N_c. $\Delta\theta/\theta_0$ versus R_0 shows behavior, intermediate between that of $\Delta R/R_0$ and $\Delta T/T_0$ because the optimized value of θ is derived by means of R and T. As a whole, $|\Delta\theta/\theta_0|$ is largest ($\approx 4\%$) for small radii and tends to zero for large radii; it is zero for zigzag tubes (by definition), intermediate for armchair tubes and largest for chiral tubes where it increases with the increase of N_c. The maximum values of the absolute changes of R, θ, and T are about 0.1 Å, 1°, and 0.4 Å, respectively. More details can be found in Ref. 29.

The trend of change of the structural parameters corresponds to the *ab initio* results for several nanotubes in Refs. 8 and 34. For example, we obtain an increase of the radius for tubes (4,4) and (10,10) of 1.6 and 0.3% compared to 1.2 and 0.2%.[34] For tubes (5,0), (3,3), and (4,2) with nonoptimized radii of 1.96, 2.03, and 2.07 Å, we obtain 2.02, 2.12, and 2.14 Å that are in fair agreement with the *ab initio* results 2.04, 2.10, and 2.14 Å. [8] The optimized nanotube structure is characterized with nonequal bond lengths and bond angles. The bond lengths and bond angles calculated here for tubes (5,0), (3,3), and (4,2) differ slightly from the corresponding *ab initio* results[8] (see Table I).

The difference between the optimized and nonoptimized structures decreases with the increase of the radius and can be ignored for large radii. It is of primary importance to study how this difference will affect the electronic band structure and the dielectric function of the nanotubes. Before proceeding further, it is interesting to compare the strain energy calculated here to the *ab initio* results.[35,34,36] Fitting the strain energy versus radius with $E_{\mathrm{st}}=C/R^2$ (Ref. 37) we obtain the value $C=2.133$ eV/atom that agrees well with 2.20 eV/atom [tubes (n,n), $n=3,\ldots,9$],[35] 2.00 eV/atom [tubes (n,n), $n=8,\ldots,12$],[36] 2.00 eV/atom [tubes (n,n), $n=4,\ldots,10$],[34] and 2.05 eV/atom [tubes (n,n), $n=4,\ldots,10$, (10,0), (8,4)].[34]

B. Electronic band structure and dielectric function

The principal goal of this work is to study the effects of (a) the choice of the atomic orbital basis set for the tight-binding model, (b) the overlap of the atomic orbitals on different atoms, and (c) the structural optimization on the electronic band structure and the dielectric function of nanotubes. The band structure and the dielectric function are calculated within the π-TB model, the *o*-TB model, and the *n*-TB model for the rolled-up structure (*n*-TB1) and the *n*-TB model for the optimized structure (*n*-TB2). For the π-TB calculations, a hopping parameter $\gamma_0=2.75$ eV was used (see, Ref. 14). The *o*-TB model implements parameters $H_{ss\sigma}=-4.80$, $H_{sp\sigma}=4.75$, $H_{pp\sigma}=4.39$, and $H_{pp\pi}=-2.56$ eV, derived by fitting to the *ab initio* band structure of graphene[38] and used in Ref. 39. The *n*-TB parametrization is the same as in Sec. III A. Since the mentioned effects are supposed to be larger for smaller-radius tubes, for better illustration, we first consider the three nanotubes (5,0), (3,3), and (4,2) with almost equal radii of ≈ 2 Å but different chirality.

First, the extension of the basis set from one $(\pi-)$ orbital to four orbitals (s, p_x, p_y, and p_z) per carbon atom and the neglect of orbital overlap corresponds to *o*-TB calculations. As seen in Fig. 1, the band structures of the three tubes within the π-TB model (dotted lines) and the *o*-TB model (full lines), differ mainly quantitatively in the values of the band energies while showing the same characteristic features: direct gaps for tubes (5,0) and (4.2), and band crossing at the Fermi energy close to $k=2/3\pi$ for tube (3,3). For all three tubes, the vertical band energy separations of the *o*-TB model are smaller than those of the π-TB model. In graphene, due to the symmetry of the sp^2 hybridized orbitals and the p orbital, oriented perpendicularly to the surface, there is no mixing between the evolving σ and π, σ^* and π^* graphene bands.[2] When graphene is rolled up into a nanotube, these bands become hybridized giving rise to modification of the *o*-TB bands relative to the π-TB ones.

Second, we consider the effects of inclusion of overlap for the rolled-up nanotube structure which corresponds to use of

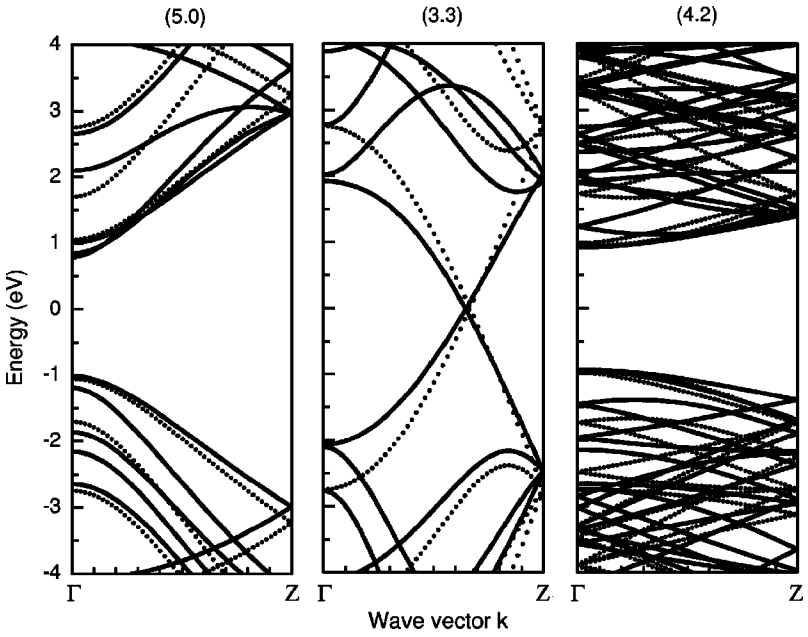

FIG. 1. Calculated electronic band structure of nanotubes (5,0), (3,3), and (4,2) in the energy range between −4 and 4 eV with respect to the Fermi energy within the *o*-TB model (full lines) and the π-TB model (dotted lines)

the *n*-TB1 model. As shown in Fig. 2, the calculated band structure within the *n*-TB1 model (full lines) exhibits major qualitative differences from that of the *o*-TB model (dotted lines). These differences can be summarized as follows: closing up of the direct gap of tube (5,0), displacing of the crossing point of the bands at the Fermi energy from $k=2/3\pi$ to $k\approx 0.4\pi$ for tube (3,3), and transforming the direct gap of tube (4,2) into an indirect one. For the three tubes there is an overall decrease of the absolute value of the band energies relative to the Fermi energy in comparison with the *o*-TB bands. The drastic changes of the band structure are due to the switching on of an additional mechanism for rehybridization through the overlap. The wrapping of the graphene sheet into a nanotube introduces nonorthogonality between the sp^2 hybridized orbitals and the *p* orbitals, oriented perpendicularly to the graphene sheet, which results in nonzero overlap. Therefore, this rehybridization mechanism is curvature-induced and will disappear in the limit of large tube radius. The dramatic improvement of the band structure upon inclusion of overlap was illustrated as well within a third nearest-neighbor nonorthogonal tight-binding model with model parameters fitted to *ab initio* data.[40]

Third, the effects of structural optimization on the band structure are investigated comparing again the results for the three small-radius tubes. It is seen in Fig. 3 that there are small differences between the *n*-TB1 and *n*-TB2 bands around the Fermi energy. This leads to the conclusion that the rolled-up nanotube structure may be used instead of the optimized one even for small-radius tubes. As a whole, the comparison between the band structures of the four models shows a clear trend for the decreasing of the vertical separation between the band energies around the Fermi energy with

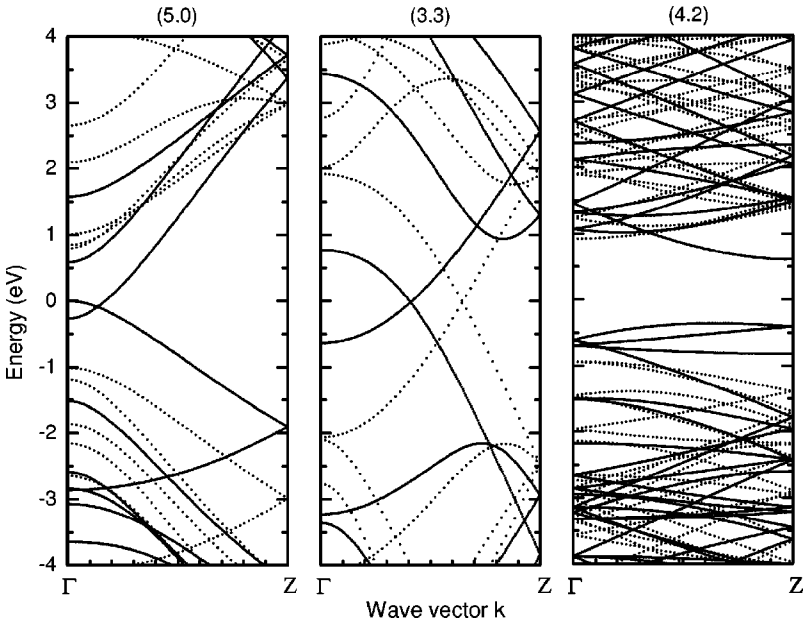

FIG. 2. Same as for Fig. 1 but for the *n*-TB1 model (full lines) and the *o*-TB model (dotted lines).

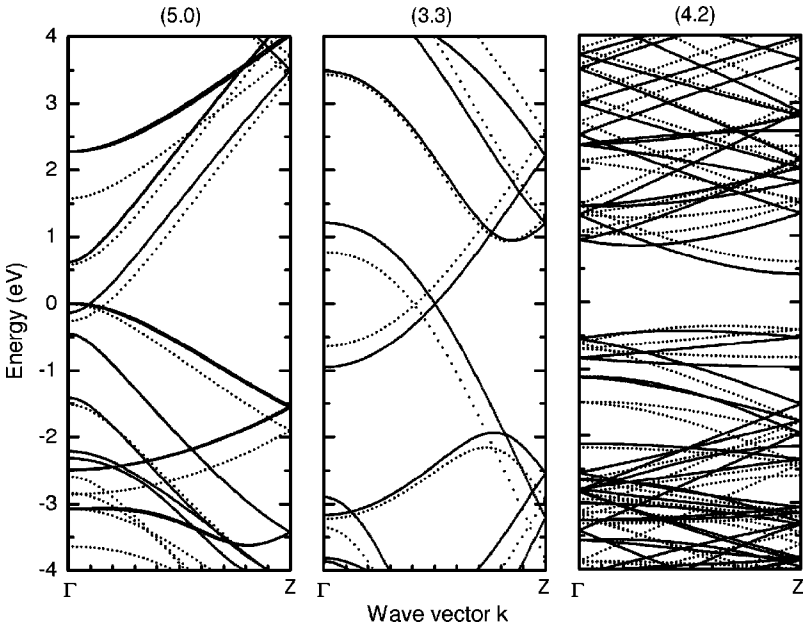

FIG. 3. Same as for Fig. 1 but for the *n*-TB2 model (full lines) and the *n*-TB1 model (dotted lines).

the improvement of the model. The *n*-TB2 results are, however, closest to previously reported *ab initio* results.[8,20] In particular, the band structure of thin tubes is modified compared to the π-TB predictions: the nanotube (5,0) is metallic, the crossing of the bands at the Fermi energy in (3,3) nanotube is at $k \approx 0.5\pi$ instead at $k=2/3\pi$, and nanotube (4,2) has an indirect band gap of 0.83 eV that is twice smaller than the π-TB direct gap but is a bit larger than the *ab initio* one.[8,20] This is an indication that the *n*-TB2 model predicts similar curvature-induced rehybridization in thin tubes as *ab initio* models.

The imaginary part of the dielectric function ε_2 of the three small-radius tubes (5, 0), (3, 3), and (4, 2) was calculated in the energy range from 0 to 6 eV with the step of 0.005 eV using a sampling of 1200 *k*-points in the numerical integration over the Brillouin zone [see, Eq. (23)]. In the *n*-TB model, the matrix element of the momentum was calculated directly while in the π-TB and *o*-TB models the basis orbitals are unknown and the gradient approximation was used. The resulting ε_2 for parallel and perpendicular polarization within the three TB models is shown in Fig. 4. The peaks for parallel polarization originate from minima and maxima of occupied and unoccupied bands with the same quantum number *l*. For example, the single peak of ε_2 for tube (3, 3) in Fig. 4 can be associated with an optical transition between a maximum of an occupied band and a minimum of an unoccupied band inside the Brillouin zone. These minima and maxima give rise to similar spikes in the electronic density of states of the nanotubes. The peaks for perpendicular polarization originate from minima and maxima of occupied and unoccupied bands or from states on parallel parts of occupied and unoccupied bands with quan-

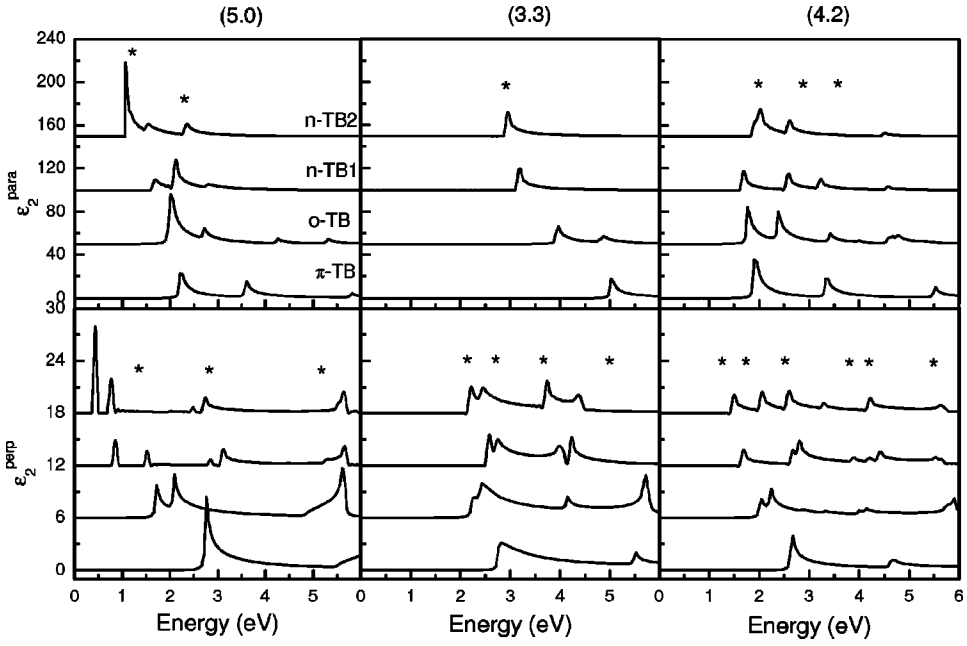

FIG. 4. Calculated dielectric function ε_2 of nanotubes (5,0), (3,3), and (4,2) for parallel and perpendicular polarization in the energy range from 0 to 6 eV within the π-TB, *o*-TB, *n*-TB1, and *n*-TB2 models. The *ab initio data* (Ref. 8) are denoted by asterisks.

tum numbers l and $l\pm1$, respectively. The comparison between the ε_2 curves of the four models shows a trend of the decreasing of transition energies upon improvement of the model by extending the basis set, including orbitals overlap, and optimizing the tube structure.

The first n-TB2 transition energies E_{11} for parallel polarization for tubes (5, 0) (1.0, 1.2 eV), (3, 3) (2.9 eV), and (4, 2) (1.85, 1.96 eV) correspond well to the LDA results 1.2, 2.9, and 1.9 eV (denoted by asterisks),[8] and 1.2, 2.9, and 2.0 eV (Ref. 9) (see Fig. 4). The smaller number of peaks in Refs. 8 and 9 is possibly due larger peak widths used in the calculations and resulting overlap of closely situated peaks. The agreement with the *ab initio* results for perpendicular polarization, which do not include depolarization effects, is good for the first optical transitions of tubes (3, 3) and (4, 2) but not for tube (5, 0). For both light polarizations, the higher-energy optical transitions deviate from the *ab initio* data for the considered very-small-radius tubes. This can be explained with the use of a small number of atomic orbitals and the neglect of three-center integrals in the derivation procedure for the n-TB parameters. Consequently, this model will describe well the effects of curvature for relatively small departures from the pure sp^2 hybridization. On the other hand, the synthesized nanotubes have normally moderate radii in which case the n-TB parameters are expected to have a better performance. It is important to stress that the predictions of the widely used π-TB models overestimate the predictions of the *ab initio* and the n-TB2 models for the three considered tubes up to two times.

It should be noted that the depolarization effects were not accounted for in the calculation of ε_2 for perpendicular polarization. On the other hand, the small lateral size of the nanotubes leads to strong depolarization effects and significant modification of the dielectric function.[11] An estimate of the depolarization field based on the classical electrodynamics exhibits that the polarization-induced correction of ε_2 diminishes with the increase of the tube radius.[11] The precise inclusion of the depolarization effects leads to a reduction of the peak height and smearing of the peaks themselves.[9] The importance of knowing the dielectric function for both parallel and perpendicular polarization has been pointed out recently in a cross-polarized resonant Raman study of nanotubes.[41]

The calculated ε_2 for 26 semiconducting tubes with $N_a<800$ for which spectrofluorimetric data exists[22] is shown in Fig. 5. It is seen in the left panel that each of the curves for parallel polarization exhibits from two to four peaks with decreasing height with the increase of the radius. The peaks originate from transitions between occupied and empty bands with the same l. The right panel presents the curves for perpendicular polarization each of which has one or two dominant peaks that come from transitions between occupied and empty bands with indices l and $l\pm1$ close to the Fermi energy. In the π-TB approach, the bands with the same l give rise to mirror spikes in the density of states and, consequently, the peaks of ε_2 from transitions $l\rightarrow l\pm1$ and $l\pm1\rightarrow l$ will coincide. Therefore, a single peak is expected to dominate each curve. The presence of two close peaks instead of a single peak can be explained with the asymmetry of the π and π^* bands of graphene relative to the Fermi

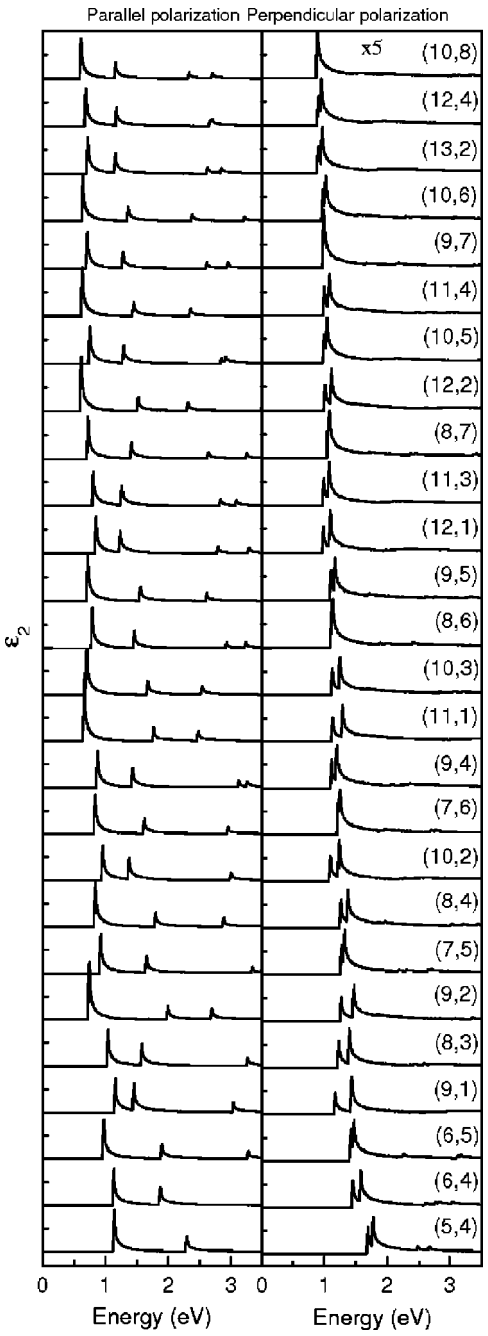

FIG. 5. Calculated dielectric function ε_2 of 26 nanotubes with $N_a<800$ (Ref. 22) for parallel and perpendicular polarization in the energy range from 0 to 3.5 eV within the n-TB2 model. The curves are arranged upwards in order of increasing tube radius from about 3.1 to 6.1Å.

energy and with the warping effect both of which are accounted for in the all-electron TB models. The peaks of ε_2 for perpendicular polarization are about five times lower than for parallel polarization.

C. Optical transition energies

Next, we study the effects of the atomic orbital basis set, orbitals overlap, and structural optimization on the dielectric

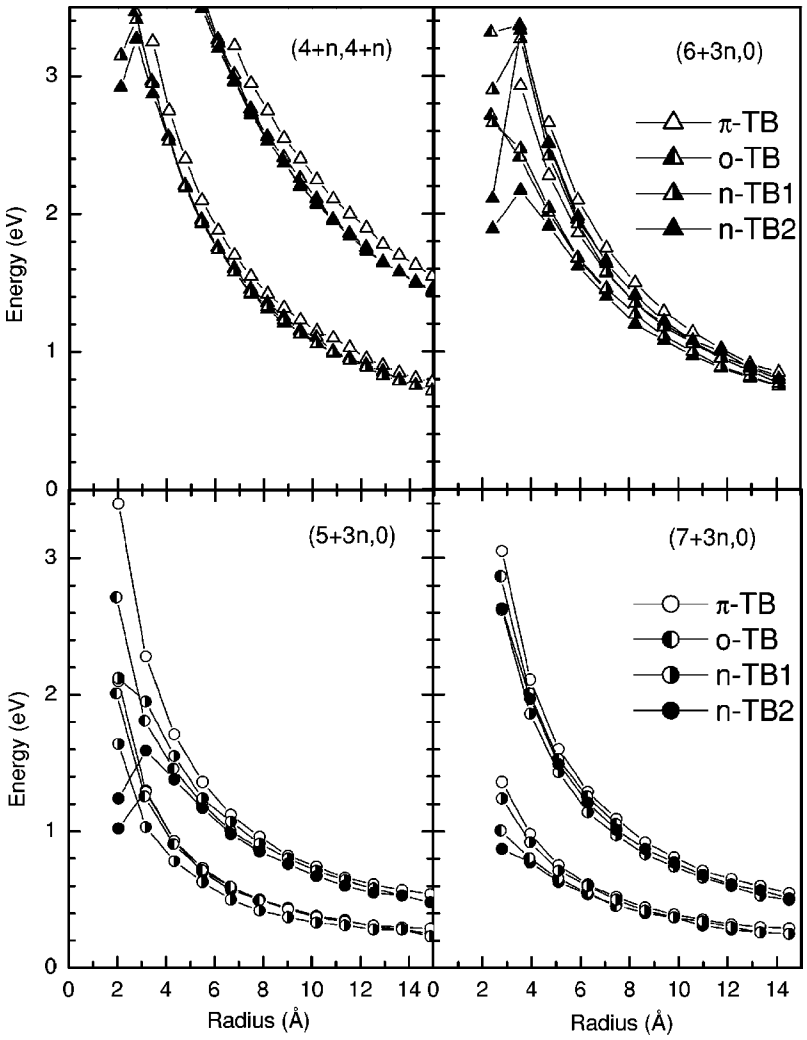

FIG. 6. Calculated optical transition energies E_{11} and E_{22} for parallel polarization versus tube radius R for all armchair and zigzag nanotubes in the range 2 Å$<R<$15 Å within the π-TB, *o*-TB, *n*-TB1, and *n*-TB2 models.

function of nanotubes within the four TB models. For better illustration of these effects, we first consider only all armchair and zigzag nanotubes in the range 2 Å$<R<$15 Å. The dielectric function was calculated as described in the previous section. The lowest two transition energies E_{11} and E_{22}, derived from the peaks of ε_2 for parallel polarization, are shown versus tube radius in Fig. 6 for the series of armchair tubes $(4+n,4+n)$ $(n=0,1,\ldots,22)$ and zigzag tubes $(5+3n,0)$, $(6+3n,0)$, and $(7+3n,0)$ $(n=0,1,\ldots,10)$. For small radii, the predictions of the four models for E_{11} and E_{22} exhibit large differences that tend to decrease with the increase of the radius. For a given tube, the transition energies of all models fall in an energy interval with width of about 0.2 eV for $R\gtrsim 7$ Å. In some cases, the *o*-TB and *n*-TB curves are downshifted by about 0.1 eV relative to the π-TB curves. These energy shifts correspond to the results of *ab initio* LDA calculations that predict downward shifts of $\sim$0.1 eV for radii in the range 5 Å$<R<$7.5 Å.[10] Most of the work on sample characterization by optical absorption and resonant Raman scattering has been based on the use of the π-TB predictions.[14] The calculations here show that the π-TB results deviate significantly from the *n*-TB ones for small-radius tubes and, consequently, the use the former may lead to misinterpretation of the absorption and Raman spectra.

Next, the optical transition energies for all nanotubes in the range 2 Å$<R<$15 Å with $N_a<800$ were derived from the peaks of ε_2. In Fig. 7, the obtained transition energies for parallel polarization within the *o*-TB and *n*-TB2 models (full symbols) are compared to the π-TB ones (empty symbols). It is clearly seen that there is a large difference between the π-TB predictions from those of the more sophisticated TB models especially for tubes with small radii. This difference decreases with the increase of the tube radius and becomes smaller than about 0.2 eV for tubes with $R\gtrsim 7$ Å in the considered energy range. The transition energies for perpendicular polarization, given in Fig. 8, are situated in a strip whose width is decreasing rapidly with the increase of the tube radius. The lowest-energy pair of peaks for any tube arises from energy bands closest to the Fermi energy. As discussed above, the appearence of pairs rather than single peaks is due to the asymmetry of the π and π^* bands of graphene and with the warping efect.

The analysis of recent absorption data on semiconducting nanotubes,[27] supported by Raman and transmission electron microscope data, revealed a large upward shift of the first transition energy E_{11} and a negligible one of the second transition energy E_{22} in comparison with the π-TB results. The curve of E_{11} versus R was fitted with a power law $R^{-1.3}$ while the π-TB model yields a R^{-1} dependence. The upshift was

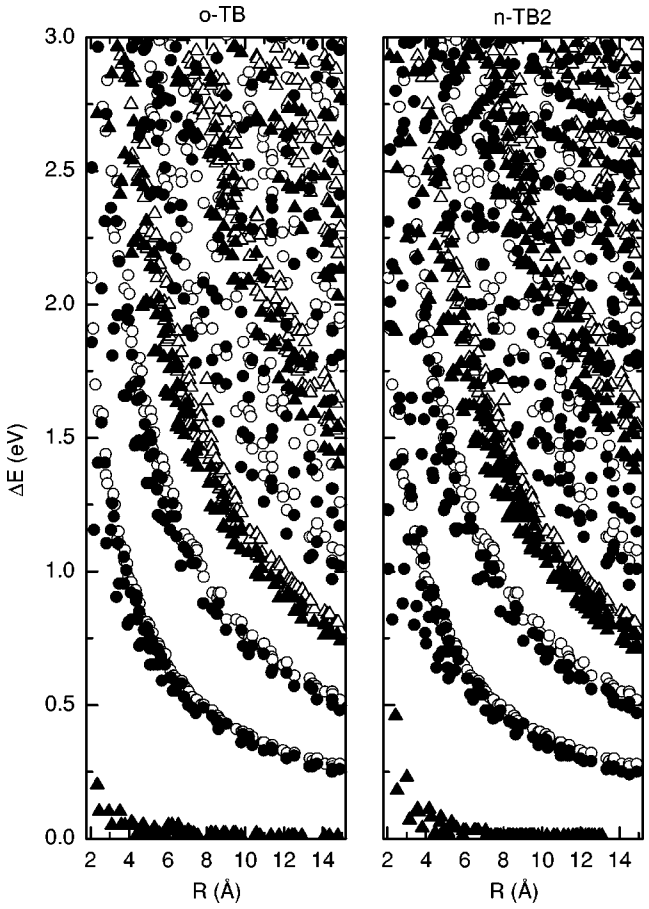

FIG. 7. Calculated optical transition energies E_{ii} for parallel polarization for all nanotubes in the range $2\ \text{Å} < R < 15\ \text{Å}$ and $N_a < 800$ within the *o*-TB model (left panel, full symbols) and the *n*-TB2 model (right panel, full symbols) in comparison with those of the π-TB model (empty symbols). Data for metallic and semiconducting tubes are designated by triangles and circles, respectively.

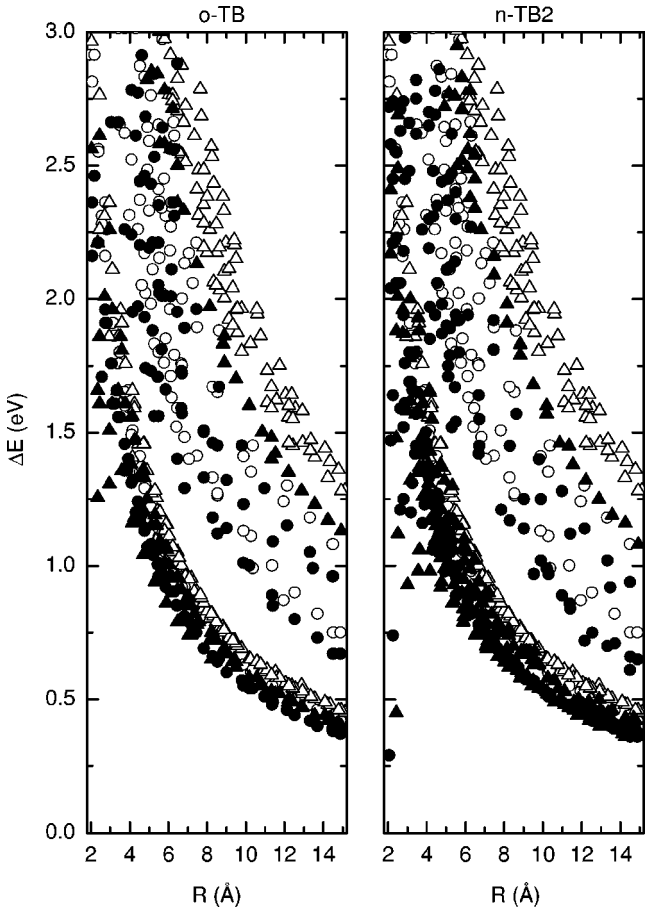

FIG. 8. Calculated optical transition energies E_{ii} for perpendicular polarization for all nanotubes as in Fig. 7.

attributed to Coulomb and excitonic effects that are not accounted for in the π-TB model.[26] Recent extensive spectrofluorimetric data on isolated semiconducting SWNTs (Refs. 22–24) were found inconsistent with the π-TB results as well. The optical transitions data for 33 tubes with $3.1\ \text{Å} < R < 6.1\ \text{Å}$ were assigned by means of power laws with chirality dependent parameters.[22,25] The observed upshift of the experimental data was attributed to effects such as the trigonal warping, curvature, and exciton binding that are not included in the π-TB picture. Since the *n*-TB2 model describes realistically the warping effect and tube curvature, the deviation of its predictions from the experimental data can be described by including self-energy and excitonic corrections. The self-energy can be approximated by a rigid shift of about 15% of the unoccupied bands with respect to the occupied ones while the excitonic corrections depend on the tube type and are generally small.[42] We chose for the purpose of comparison the spectrofluorimetric data for all 26 tubes with $N_a < 800$ from Ref. 22 for which ε_2 is plotted in Fig. 5. It is seen in Fig. 9 that the *n*-TB2 points, when shifted upward by 0.3 eV, coincide well with the experimental data for E_{11} and E_{22} with deviations below 0.05 eV. It is evident from Fig. 9 that the π-TB data cannot be coincided with the experimental ones by means of any chirality independent shift. The comparison of the *n*-TB2 points with the transition energies for all 59 tubes with $N_a < 800$ and radii up to 10 Å from Ref. 25 shows that the upshift decreases with the increase of the radius and has values of about 0.2 eV for radii close to 10 Å. Such a behavior of the upshift is consistent with the finding that the increase of the transition energies in nanotubes in comparison with the band structure ones is a consequence of the spatial confinement of the electrons in them and that this increase should be smaller for larger radii.[26] It can be concluded that the upshift is mainly due to self-energy corrections since it is in the range of these corrections. This conclusion does not rule out a possible excitonic contribution. A recent analysis of the dynamics of the photoexcitations spectra of carbon nanotube films is in favor of the excitonic character of the optical transitions in carbon nanotubes.[43] The precise determination of the radius and chirality dependence of the exciton shift can be done only within a theory of the excitonic effects in nanotubes, which goes beyond the band structure picture and the goal of this paper.

IV. CONCLUSIONS

Orthogonal and nonorthogonal tight-binding models are used for band structure and optical transitions calculations of

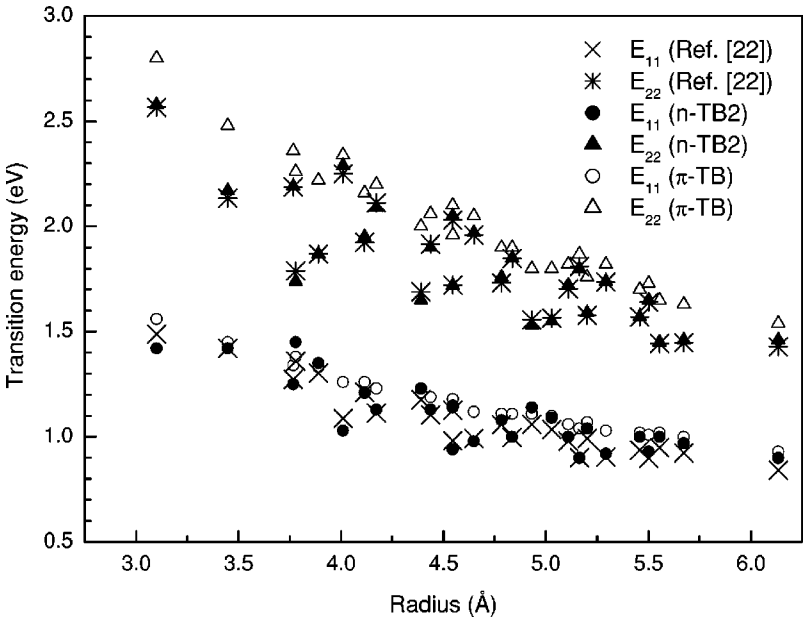

FIG. 9. Comparison between spectrofluorimetric data on SWNTs for the transition energies E_{11} and E_{22} (Ref. 22) and corresponding π-TB and *n*-TB2 results shifted up uniformly by 0.3 eV. It is clearly seen that the latter points coincide well with the experimental data. The upward shift can be attributed to self-energy and excitonic effects that are not included in the band structure picture.

a large number of single-walled carbon nanotubes. The models implement a symmetry-adapted scheme which allows for a significant reduction of the size of the matrix electronic eigenvalue problem and is advantageous with respect to computational time and resources over the nonsymmetry-adapted models. The models are used to study the effects of the orbital basis set, orbitals overlap, and structural optimization. The calculated electronic band structure and dielectric function of three small-radius relaxed nanotubes within the nonorthogonal tight-binding model agree well with *ab initio* LDA simulations. The optical transition energies of all 187 nanotubes with radii in the range $2\ \text{Å} < R < 15\ \text{Å}$ and $N_a < 800$ nanotubes are calculated and compared to the π-TB predictions. It is shown that the calculated transition energies, upshitted by 0.3 eV, coincide well with available spectrofluorimetric data on nanotubes. This shift can be attributed mainly to self-energy corrections to the electronic energies.

ACKNOWLEDGMENTS

V.N.P. was partly supported by a scholarship from the Belgian Federal Science Policy Office for promoting the S&T cooperation with Central and Eastern Europe and Grant MEIF-CT-2003-501080 within the 6th European Community Framework Programme. L.H. was supported by the Belgian National Fund (FNRS). This work was partly funded by the Belgian Interuniversity Research Project on quantum size effects in nanostructured materials (PAI-UAP P5-1). V.N.P. and L.H. were partly supported by a NATO Collaborative Linkage Grant No. 980422.

*Permanent address: Faculty of Physics, University of Sofia, BG-1164 Sofia, Bulgaria.

[1] S. Iijima, Nature (London) **354**, 56 (1991).

[2] *Carbon nanotubes: Synthesis, Structure, Properties, and Applications*, edited by M. S. Dresselhaus, G. Dresselhaus, and Ph. Avouris (Springer-Verlag, Berlin, 2001).

[3] R. Saito, M. Fujita, G. Dresselhaus, and M. S. Dresselhaus, Phys. Rev. B **46**, 1804 (1992).

[4] N. Hamada, S. I. Sawada, and A. Oshiyama, Phys. Rev. Lett. **68**, 1579 (1992).

[5] J. W. Mintmire, D. H. Robertson, and C. T. White, J. Phys. Chem. Solids **54**, 1835 (1993).

[6] X. Blase, L. X. Benedict, E. L. Shirley, and S. G. Louie, Phys. Rev. Lett. **72**, 1878 (1994).

[7] J.-C. Charlier, Ph. Lambin, and T. W. Ebbesen, Phys. Rev. B **54**, R8377 (1996).

[8] M. Machón, S. Reich, C. Thomsen, D. Sánchez-Portal, and P. Ordejón, Phys. Rev. B **66**, 155410 (2002).

[9] A. G. Marinopoulos, L. Reining, A. Rubio, and N. Vast, Phys. Rev. Lett. **91**, 046402 (2003).

[10] S. Reich, C. Thomsen, and P. OrdejÓn, Phys. Rev. B **65**, 155411 (2002).

[11] H. Ajiki and T. Ando, Physica B **201**, 349 (1994).

[12] M. F. Lin and Kenneth W.-K. Shung, Phys. Rev. B **50**, 17744 (1994).

[13] S. Tasaki, K. Maekawa, and T. Yamabe, Phys. Rev. B **57**, 9301 (1998).

[14] H. Kataura, Y. Kumazawa, Y. Maniwa, I. Umezu, S. Suzuki, Y. Ohtsuka, and Y. Achiba, Synth. Met. **103**, 2555 (1999).

[15] A. Hagen and T. Hertel, Nano Lett. **3**, 383 (2003).

[16] J. X. Cao, X. H. Yan, J. W. Ding, and D. L. Wang, J. Phys.: Condens. Matter **13**, L271 (2001).

[17] I. Milošević, T. Vuković, S. Dmitrović, and M. Damnjanović, Phys. Rev. B **67**, 165418 (2003).

[18] J. Hwang, H. H. Gommans, A. Ugawa, H. Tashiro, R. Haggenmueller, K. I. Winey, J. E. Fischer, D. B. Tanner, and A. G.

Rinzler, Phys. Rev. B **62**, R13310 (2000).
[19] X. Liu, T. Pichler, M. Knupfer, M. S. Golden, J. Fink, H. Kataura, and Y. Achiba, Phys. Rev. B **66**, 045411 (2002).
[20] Z. M. Li, Z. K. Tang, H. J. Liu, N. Wang, C. T. Chan, R. Saito, S. Okada, G. D. Li, J. S. Chen, N. Nagasawa, and S. Tsuda, Phys. Rev. Lett. **87**, 127401 (2001).
[21] M. J. O'Connell, S. M. Bachilo, C. B. Huffman, V. C. Moore, M. S. Strano, E. H. Haroz, K. L. Rialon, P. J. Boul, W. H. Noon, C. Kittrell, J. Ma, R. H. Hauge, R. B. Weisman, and R. E. Smalley, Science **297**, 593 (2002).
[22] S. M. Bachilo, M. S. Strano, C. Kittrell, R. H. Hauge, R. E. Smalley, and R. B. Weisman, Science **298**, 2361 (2002).
[23] A. Hartschuh, H. N. Pedrosa, L. Novotny, and T. D. Krauss, Science **301**, 1354 (2003).
[24] S. Lebedkin, F. Hennrich, T. Skipa, and M. M. Kappes, J. Phys. Chem. **107**, 1949 (2003).
[25] R. B. Weisman and S. M. Bachilo, Nano Lett. **3**, 1235 (2003).
[26] T. Ando, J. Phys. Soc. Jpn. **66**, 1066 (1997).
[27] M. Ichida, S. Mizuno, Y. Saito, H. Kataura, Y. Achiba, and A. Nakamura, Phys. Rev. B **65**, 241407 (2002).
[28] V. N. Popov, V. E. Van Doren, and M. Balkanski, Phys. Rev. B **59**, 8355 (1999); *ibid.* **61**, 3078 (2000).
[29] V. N. Popov, New J. Phys. **6**, 17 (2004).
[30] H. Ehrenreich and M. H. Cohen, Phys. Rev. **115**, 786 (1959).
[31] G. Dresselhaus and M. S. Dresselhaus, Phys. Rev. **160**, 649 (1967).
[32] T. G. Pedersen, K. Pedersen, and T. B. Kriestensen, Phys. Rev. B **63**, 201101 (2001).
[33] D. Porezag, Th. Frauenheim, Th. Köhler, G. Seifert, and R. Kaschner, Phys. Rev. B **51**, 12947 (1995).
[34] D. Sánchez-Portal, E. Artacho, J. M. Soler, A. Rubio, and P. Ordejón, Phys. Rev. B **59**, 12678 (1999).
[35] D. H. Robertson, D. W. Brenner, and J. W. Mintmire, Phys. Rev. B **45**, 12592 (1992).
[36] J. Kürti, G. Kresse, and H. Kuzmany, Phys. Rev. B **58**, R8869 (1998).
[37] G. Adams, O. Sankey, J. Page, M. O'Keeffe, and D. Drabold, Science **256**, 1792 (1992).
[38] J.-C. Charlier, X. Gonze, and J.-P. Michenaud, Phys. Rev. B **43**, 4579 (1991).
[39] A. A. Lucas, Ph. Lambin, and R. E. Smalley, J. Phys. Chem. Solids **54** 587 (1992).
[40] S. Reich, J. Maultzsch, C. Thomsen, and P. Ordejón, Phys. Rev. B **66**, 035412 (2002).
[41] A. Jorio, M. A. Pimenta, A. G. Souza Filho, Ge. G. Samsonidze, A. K. Swan, M. S. Ünlü, B. B. Goldberg, R. Saito, G. Dresselhaus, and M. S. Dresselhaus, Phys. Rev. Lett. **90**, 107403 (2003).
[42] C. D. Spataru, S. Ismail-Beigi, L. X. Benedict, and S. G. Louie, Phys. Rev. Lett. **92**, 077402 (2004).
[43] O. J. Korovyanko, C.-X. Sheng, Z. V. Vardeny, A. B. Dalton, and R. H. Baughman, Phys. Rev. Lett. **92**, 017403 (2004).